Scientific Paper / Artículo Científico

UNIVERSIDAD POLITÉCNICA SALESIANA ECUADOR
INGENIUS
Revista de Ciencia y Tecnología
https://doi.org/10.17163/ings.n33.2025.04
pISSN: 1390-650X / eISSN: 1390-860X

Prototype of a remotely controlled multichannel surface muscle stimulator

Prototipo de estimulador muscular superficial multicanal controlado remotamente

P. Silverio-Cevallos[1,*], J. Maita Cajamarca[1], D. A. Molina-Vidal[2], C. J. Tierra-Criollo[2], P. Cevallos-Larrea[1]

Received: 13-11-2023, Received after review: 29-05-2024, Accepted: 05-11-2024, Published: 01-01-2025

Abstract

Multichannel Functional Electrical Stimulation (FES) technology is widely employed in artificial motor control research. This study presents the design and evaluation of a four-channel, remotely controlled surface electrical muscle stimulator prototype. The prototype introduces a modern alternative for the control block, employing a Wi-Fi-enabled solution based on the ESP32 microcontroller. This controller enables remote configuration of activation sequences for individual channels and supports extensive customization of parameters for a biphasic waveform stimulus. The current signal is demultiplexed into four outputs. Additionally, this study provides a detailed functional evaluation of the amplification stage and examines the load-dependent limitations of the output current magnitude. Preliminary experimental testing demonstrates the prototype's ability to generate controlled stimulation sequences in hand muscles. The prototype's functional and experimental performance suggests its potential application in artificial motor control research.

Keywords: Multichannel Functional Electrical Stimulator, Muscle Stimulator, Artificial Motor Control

Resumen

La tecnología de Estimulación Eléctrica Funcional (EEF) multicanal se utiliza actualmente en la investigación del control motor artificial. Este trabajo describe el diseño y evaluación de un prototipo de estimulador eléctrico muscular de cuatro canales controlado remotamente. El prototipo propone una alternativa moderna para el bloque de control, utilizando el microcontrolador Wi-Fi/ESP32. Este permite una secuencia de activación de canales configurable de manera remota y una extensiva configuración de los parámetros de un estímulo en forma de onda bifásica. La señal de corriente se demultiplexa en cuatro salidas. Este estudio también contribuye detallando la evaluación funcional de la etapa de amplificación y estableciendo la dependencia de la magnitud de la carga en los límites de la corriente de salida. La prueba experimental preliminar demuestra la capacidad del prototipo para generar secuencias de estimulación controladas en los músculos de la mano. El desempeño funcional y experimental del prototipo sugiere su potencial uso para investigaciones del control motor artificial.

Palabras clave: Estimulador Eléctrico Funcional Multicanal, Estimulador Muscular, Control Motor Artificial

[1,*]Biomedical Engineering Research Group - GIIB, Universidad Politécnica Salesiana, Ecuador.
Corresponding author ✉: psilverio@est.ups.edu.ec.
[2] Biomedical Engineering Program, Alberto Luiz Coimbra Institute for Graduate Studies and Research in Engineering (Coppe), Federal University of Rio de Janeiro, Brazil.

Suggested citation: Silverio-Cevallos, P., Maita Cajamarca, J., Molina-Vidal, D. A., Tierra-Criollo, C. J. and Cevallos-Larrea, P. "Prototype of a remotely controlled multichannel surface muscle stimulator," *Ingenius, Revista de Ciencia y Tecnología*, N.° 33, pp. 38-48, 2025, DOI: https://doi.org/10.17163/ings.n33.2025.04.

1. Introduction

Neurodegenerative disorders, such as Parkinson's disease (PD), spinal muscular atrophy, and amyotrophic lateral sclerosis, among others [1–3], have a profound impact on the nervous system, frequently affecting motor functions. Common symptoms associated with these motor disorders include difficulty initiating and coordinating smooth muscular movements, inhibition of involuntary movements, challenges with postural adjustment, progressive limb muscle weakness, and muscle atrophy [4–6].

Electrical stimulation therapy plays a pivotal role as a non-pharmacological treatment for motor disorders associated with neurodegenerative diseases. Common non-invasive techniques include Transcutaneous Electrical Nerve Stimulation (TENS) and Functional Electrical Stimulation (FES). TENS primarily targets afferent nerve fibers to mitigate muscle atrophy, alleviate pain, enhance muscle strength, and support functional movement therapy [7]. In contrast, FES stimulates motor nerves to induce contractions in weak or paralyzed muscles. This technique is particularly effective for patients with motor impairments, such as those experiencing paralysis or severe muscle weakness [8].

Artificial motor control through FES is an assistive strategy designed to achieve functional and intentional movements by inducing controlled contractions in targeted muscle groups [9]. The therapeutic potential of this technique has been extensively studied in various conditions, including Parkinson's disease [10], paraplegia [11] and neuroprosthetics [12].

Research conducted by Qi Wu et al. [13] and Masdar et al. [14] demonstrated the efficacy of electrical stimulation in restoring and maintaining muscle activity in paralyzed patients with spinal cord injuries and related neural deficits. Furthermore, studies by Hai-Peng Wang et al. [15] and Keller T. [16] highlighted the use of electrical stimulation to enhance motor control and support motor function training in stroke patients.

Despite the availability of various commercial electrical stimulation technologies, experimental paradigms in artificial motor control often require stimulators with capabilities that surpass those offered by standard TENS and FES technologies [17, 18]. For instance, advanced features such as multichannel stimulation with remotely programmable output patterns and customizable stimulus parameters are critical in this context [19].

However, detailed accounts of such advanced electrical stimulation prototypes remain limited. One notable example is the multichannel programmable stimulator prototype developed by Qi Xu et al. [20].

Similarly, Hai-Peng Wang et al. [15] proposed a FES stimulator capable of multiplexing signals from an amplifier circuit across multiple outputs with programmable stimuli. Despite these advancements, current reports on multichannel electrical stimulation technology for complex motor control exhibit significant limitations [15], [20].

First, many prior studies rely on electronic control blocks that are difficult to procure or replicate due to inaccessible developer tools and documentation [15], [19]. For instance, the prototypes described in [15], [20] employ outdated controller technologies.

Second, these reports often lack comprehensive descriptions of performance evaluations and the limitations of signal amplification and current source circuitry, impeding reproducibility and validation efforts.

To address the need for contrasting and replicable research in advanced motor control, it is essential to explore modern and easily replicable technologies for electrical stimulation. This study aims to design and evaluate a prototype multichannel, wireless surface electrical stimulator for FES. The design specifications include remote control functionality via a smartphone and the use of widely available electronic components with extensive development resources to facilitate replication.

Additionally, the prototype is capable of generating programmable sequences of multiplexed rectangular biphasic signals across four isolated channels. The controller block is implemented using the ESP32 wireless microcontroller, a widely adopted platform known for its large support community, versatility, and scalability [21–24].

Furthermore, a preliminary experimental test was conducted to assess the prototype's ability to generate sequential, programmable muscle contractions in hand muscles, captured using a sensorized glove equipped with accelerometers.

2. Materials and methods

2.1. Design Methodology

Figure 1 illustrates the general architecture of the Multichannel Surface Electrical Stimulator (MSES). The system consists of two primary components: (i) a hardware module that generates biphasic waveform current stimuli across four asynchronously activated channels, and (ii) a software module, implemented as a smartphone application, which allows users to configure stimulation parameters, including magnitude, total period, inter-stimulus interval, and stimulation sequences across output channels. Communication between the hardware and software modules is facilitated through a wireless (Wi-Fi) connection.

2.2. Hardware

The hardware architecture consists of three main blocks: sourcing, control, and current stimulus generation, as depicted in Figure 2.

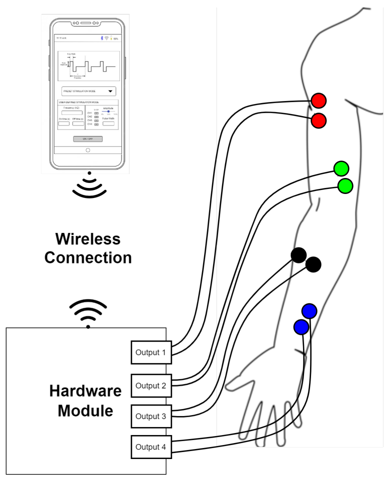

Figure 1. General architecture of the MSES

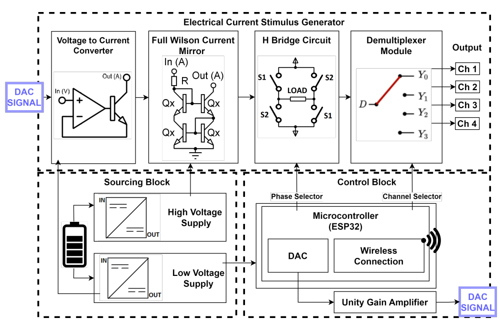

Figure 2. Hardware architecture of MSES

The Sourcing Block is powered by a 5 VDC battery, generating two isolated voltage levels. A low voltage level of +/- 5 VDC is provided by an isolated DC-DC converter (model THM 10-0521WI) to power the digital circuits within the control block and the analog signal conditioning circuit in the initial stage of the current stimulus generator. Additionally, ahigh voltage level of +/- 60 VDC is generated using an isolated DC-DC converter (model R05-100B) to supply the current stimulus generator.

The Control Block is managed by an ESP32 microcontroller (Ten silica Xtensa, 32-bit, LX6 processor), featuring integrated wireless communication capabilities. The firmware algorithm processes incoming commands—such as start, stop, update stimulus, and channel sequence—as well as stimulus parameters, including anodic and cathodic current periods, magnitude, and inter-channel intervals, from the remote application. The control block sets the low-level stimulus amplitude using an 8-bit digital-to-analog converter (DAC) connected to a unity-gain amplifier circuit, providing a DAC output range of 0 to 3.3 VDC. Additionally, it performs two critical functions within the current stimulus generator block: reversing the amplified magnitude of the electrical pulse to produce a biphasic stimulus and demultiplexing the stimulus to a designated output channel.

The Electrical Current Stimulus Generator comprises four main stages. The first stage converts the low-level voltage from the DAC signal into a high-voltage-driven current signal (+/-60 VDC), adhering to the recommendations outlined in [15]. Specifically, the DAC signal is fed into a voltage-to-current converter circuit, commonly referred to as a transconductance amplifier. The resulting current signal drives two current amplification circuits (Wilson Current Mirror - WCM), each powered by the levels HV+ and HV-, creating a constant current flow through OUT+ and OUT- when a load is connected, as depicted in Figure 3. In the WCM circuit, using resistor values (R+ and R-) lower than 1 $k\Omega$ results in signal degradation at the output, particularly for of $\approx 1k\Omega$. This study adopted resistor values of 2.4 $k\Omega$ for R+ and R-, which demonstrated the lowest noise levels at the output and minimized voltage drop across VCE in transistors Q1 and Q2. The specific values of R+ and R- also influence the maximum voltage at OUT+ and OUT-, consequently limiting the maximum current output [15].

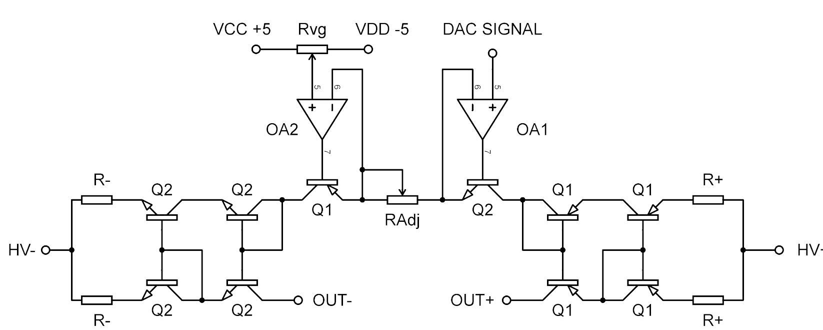

Figure 3. Electrical Schematic of the Voltage-to-Current Converter (V-to-C) Circuit and the Wilson Current Mirror (WCM) Circuits. The V-to-C circuit uses Op Amps TLC2252 (OA1 and OA2) and a variable resistor (RAdj) to adjust the working current range. The WCM employs NPN transistors (2N6517, Q2) with resistor R- to amplify the signal to HV-, and PNP transistors (2N6520, Q1) with resistor R+ to achieve HV+

In the second stage, the output terminal of the WCM is connected to a phase inverter circuit featuring a programmable four-switch H-bridge topology controlled by the control block. This circuit reverses the direction of current flow through the load to generate a biphasic waveform or disables stimulus transmission entirely. The hardware can be configured to produce a square waveform with specified durations for the anodic cycle (anodic current, S1 switches ON), cathodic cycle (cathodic current, S2 switches ON), and the interval between these cycles. Finally, the biphasic signal passes through a selector circuit (demultiplexer) that, based on the configuration of the control block, directs the stimulus to one of the four available outputs.

2.3. Software

This project utilized the Modular platform to develop a smartphone-based user interface application, as depicted in Figure 4 [25]. The application enables users to adjust stimulus parameters (Figure 4a), including stimulus magnitude (I+, I-), total period (T), anodic current period (Tp, positive), cathodic current period (Tn, negative), and two unstimulated periods: Tc1 (between Tp and Tn) and Tc2 (following Tn).

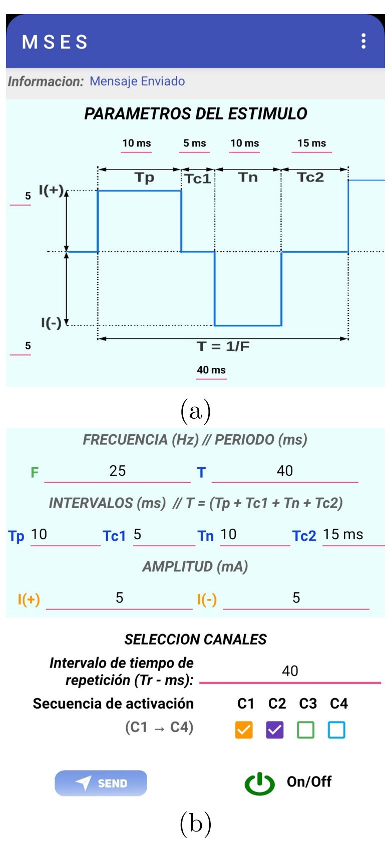

Figure 4. User Interface Application. (a) Waveform panel displaying stimulus parameters. (b) Controls for inputting stimulus parameters and managing the stimulation protocol

When stimulation is applied to a specific channel, the stimulus is delivered repeatedly to that output over a user-configurable period, Tr, ensuring consistent mechanical contractions that may not be achievable with a single square stimulus pulse. The user interface supports real-time updates of stimulation parameters in the hardware and manages the application of stimuli (Figure 4b).

During multichannel stimulation, the configured stimulus is sequentially directed to the enabled channels in ascending order(i.e., from channel 1 to channel 4).

2.4. Performance Tests

The evaluation of the system's performance involves determining the operational limits of the stimulus parameters and the multichannel stimulation paradigm. The first test assessed the stimulus magnitude by activating a single output (channel 1) and varying both the stimulus magnitude and the resistive load values (1 $k\Omega$, 5 $k\Omega$, and 10 $k\Omega$). During this test, the DAC output was set to nine fixed values within its dynamic range, enabling the derivation of an equation relating the digital values configured in the DAC to the output current levels. The second test measured the stability of the electrical current and the rising and falling times of the square wave stimulus under varying load conditions. The test used a fixed current level of 5 mA, with period values for Tp, Tn, Tc1, Tc2, and total period (T) set to 25 ms, 25 ms, 10 ms, 40 ms, and 100 ms, respectively (F = 10 Hz). Resistive load values of 1, 3.3, 5.6, 10, 12, and 20 $k\Omega$ were applied. The final test evaluated the system's capability to sequentially redirect the configured stimulus across multiple channels, following the multichannel stimulation paradigm. This test simultaneously measured two channels (channels 1 and 2), using stimulus magnitudes of 2.5 mA and 5 mA, periods Tp and Tn of 25 ms and 40 ms, respectively, and a Tr period equal to the total period T (one stimulus per channel).

2.5. Preliminary application test

This preliminary application test served as an initial evaluation of the proposed technology, without extensive testing on healthy individuals or patients with neurodegenerative diseases. The primary objective was to assess the system's ability to generate controlled electrical current stimuli across multiple channels, inducing intentional finger contractions in a predetermined sequence. The experiment was conducted in the Laboratory of the Biomedical Engineering Research Group (GIIB-UPS) with two participants, both authors of this study. Both participants reported being in good health, with no history of muscular or neurological disorders, cardiac conditions, or pacemaker use. This test adhered to the ethical principles outlined in the Declaration of Helsinki [26], and informed consent was obtained from both participants. Three stimulation regions (R1, R2, R3) on the forearm and a ground region (RG) on the olecranon were identified for electrode placement (Figure 5a). This configuration followed a previously established protocol [27] to elicit contractions in the index, middle, and ring + little fingers, corresponding to stimulation in R1, R2, and R3, respectively.

Before initiating multichannel stimulation, the stimulus magnitude was determined to elicit visible but painless muscular contractions. To achieve this, single-channel stimulation was applied, gradually increasing the current level from 0 mA until a visible contraction was observed, ensuring the absence of pain for the participant. The parameters selected for the multichannel test were as follows: total period (T) of 20 ms, anodic (Tp) and cathodic (Tn) phases of 200 μs, an interphase interval (Tc1) of 100 μs, a repetition interval (Tr) of 5 s, and a stimulus magnitude of approximately 5 mA. These stimulation levels align with those used in previous studies [28].

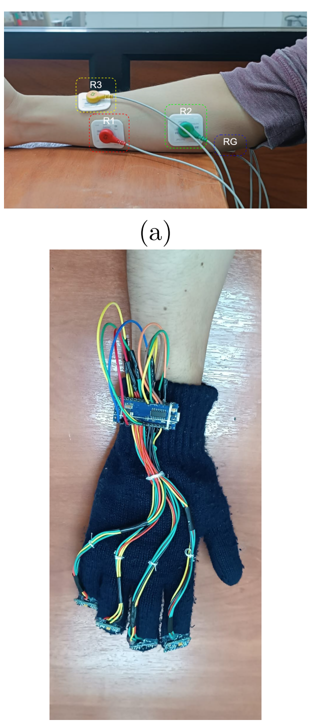

(a)

(b)

Figure 5. (a) Electrode placement regions for forearm stimulation(R1, R2, R3) and reference in RG., (b) Sensing glove with MPU6050 sensors attached to index, middle, ring, and little fingers

For multichannel stimulation, three channels (C1, C2, C3) and two stimulation modes were utilized. In the first mode, channels C1, C2, and C3 were connected to regions R1, R2, and R3, respectively. In the second mode, the connections were reconfigured to R2, R3, and R1, respectively. In both modes, the stimulator was programmed with a sequential stimulation pattern of $C1 \rightarrow C2 \rightarrow C3$.

A sensing glove was developed to objectively measure finger movement in response to each stimulus. This glove incorporates four acceleration sensors (MPU6050), each attached to the index, middle, ring, and little fingers (Figure 5b). The sensors communicate with an AT mega 328 microcontroller (Arduino Nano) via the I2C protocol, and the recorded data are stored in a digital .txt file using serial communication. The sensor data facilitate the calculation of the rotation angle (pitch) for each finger as it flexes. Before stimulation, the participant was instructed to maintain their hand in a natural, relaxed position (rest), during which the initial mean rotation angles were recorded. Consequently, the sensor data are expressed as values relative to the sensors initial positions.

3. Results and discussion

3.1. Performance Indicators

The DAC's output varied linearly within a range of -0.08 to 2.93 V for input values between 0 and 255 digital units. To achieve a 10 mA output in the electric current generator block from the maximum DAC output voltage, RAdj in the V-to-C circuit (Figure 3) was set according to the equation: $RAdj = VDAC_{max}/I_{max}$, that is $2.93V/10mA = 293\Omega$. RAdj adjusts the current level at the output of the V-to-C circuit, which is subsequently amplified through the WCM circuit (Figure 3). Figure 6a illustrates a directly proportional relation between the voltage across the load and the DAC levels. The output voltage increases with the load value to maintain a fixed current level at the output. However, as the load magnitude increases, both the output voltage and the current level reach saturation. This behavior is attributed to the maximum voltage available at the OUT+/− terminals during the performance test, which reached a maximum value of 77.6 VDC. It is important to note that during experimental tests, the DC-DC converters were set to provide+/-64 V for +/-HV. Figure 6b demonstrates an approximately linear relationship between the output current and the DAC control variable for three resistive loads (1, 5, and 10 $k\Omega$). A maximum current of 7.63 mA was achieved for the 10 $k\Omega$ load, consistent with the saturation explanation provided earlier. For the 5 $k\Omega$ load, the linear trend was calculated using least-squares regression to determine the output/input relationship. This analysis yielded the equation: $I_{out}(mA) = (0.038\times$ digital value$)$ -0.0819, is integrated into the firmware algorithm to convert the stimulus magnitude, expressed in units of electric current, into digital DAC values: digital value $= (1000 \times I_{out} + 81.9)/38.8$.

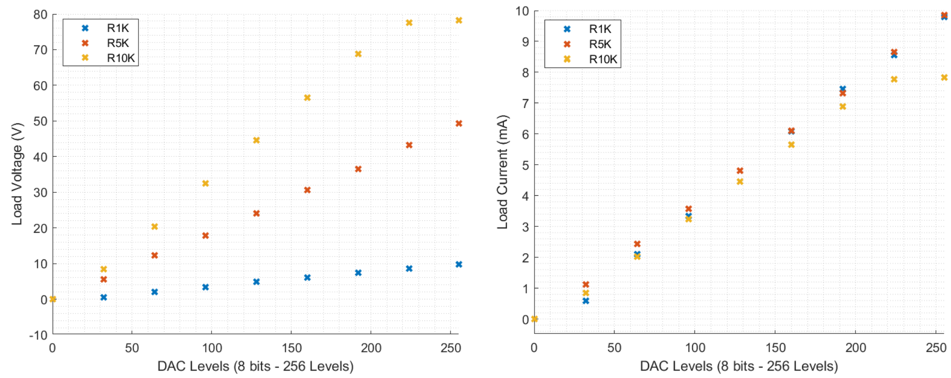

(a) (b)

Figure 6. Voltage and current measurements for a single stimulus applied to resistive loads of 1, 5, 10 $k\Omega$, within the range of the DAC control variable. (a) Load output voltage vs DAC Levels, (b) Load output current vs DAC Levels

Figure 7a illustrates the waveform of the output current signal for load resistances ranging from 1 $k\Omega$ to $k\Omega$. Overall, the measured magnitude of the biphasic stimulus remains stable, with a mean value of 4.38 mA and a standard deviation of +/- 618 μ A (12.37 % relative to the stimulus magnitude). The maximum variation (14.5 %) was observed at a load of 20 $k\Omega$. Figure 7b depicts the signal transition time measurements for changes between stimulus magnitudes of 10 % to 90 % and vice versa. The average rise time was 10.1 μs, with minimum and maximum times of 1.6 μ s and 11.7 μ s, respectively. Some non-linearities in signal magnitude, such as a peak at the start of the transition, were noted as the load resistance decreased. Conversely, the average fall time was 10.9 μ s, with minimum and maximum times of 0.4 μ s and 11.3 μ s, respectively. In general, both rise and fall times increased slightly as the load resistance increased.

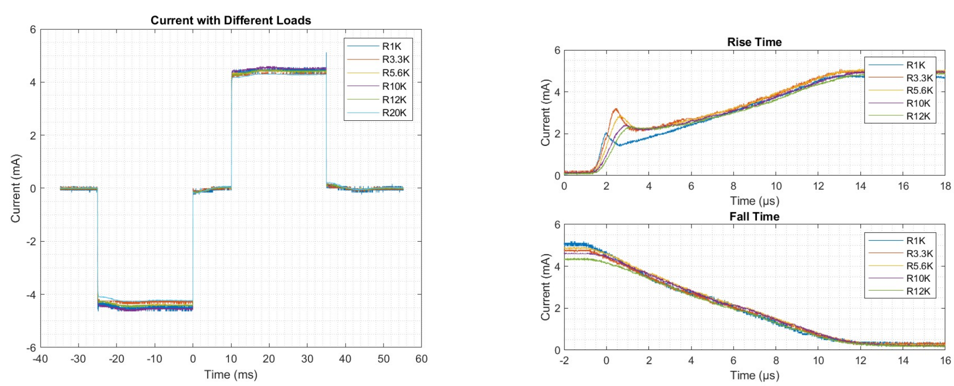

(a) (b)

Figure 7. Stimulus waveform parameters for different load resistances: (a) Stability of the biphasic stimulus waveform current, (b) Rise and fall times for a stimulus magnitude of 5 mA

Names should be abbreviated using initials only. The amplitudes and periods generated by the MSES closely matched those configured in the user interface, as shown in Figure 8. This figure illustrates a sequence of stimuli generated on channels one and two, with variations in some stimulus parameters. In Figure 8a, the values for Tp, Tn, and magnitude were 40 ms, 40 ms, and 2.72 mA, respectively, while in Figure 8b, these values were 25 ms, 25 ms, and 5.26 mA. The total period (T), which was set equal to Tr for this test, was 100 ms. Additionally, Figure 8 demonstrates the absence of interchannel interference during sequential stimulation on channels one and two.

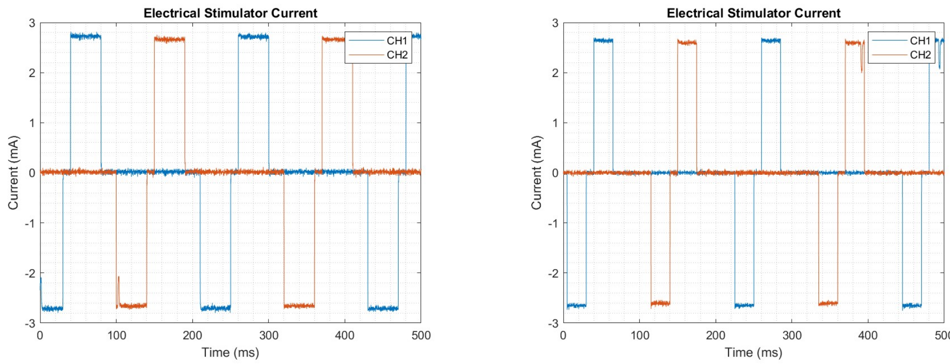

(a) (b)

Figure 8. Output of two synchronously applied channels. (a) signal with Tp and Tn of 40 ms and (b) signal Tp and Tn of 25 ms.

3.2. Application test

Finger contraction and relaxation events, along with their relationship to the two proposed stimulation sequences, were analyzed using the signals recorded by the sensorized glove for participants #1 and #2 (Figure 9). Overall, the sensor data demonstrated that specific finger movement patterns are primarily influenced by the stimulated region, with less influence from the stimulation sequence ($R1 \rightarrow R2 \rightarrow R3$ or $R2 \rightarrow R3 \rightarrow R1$).

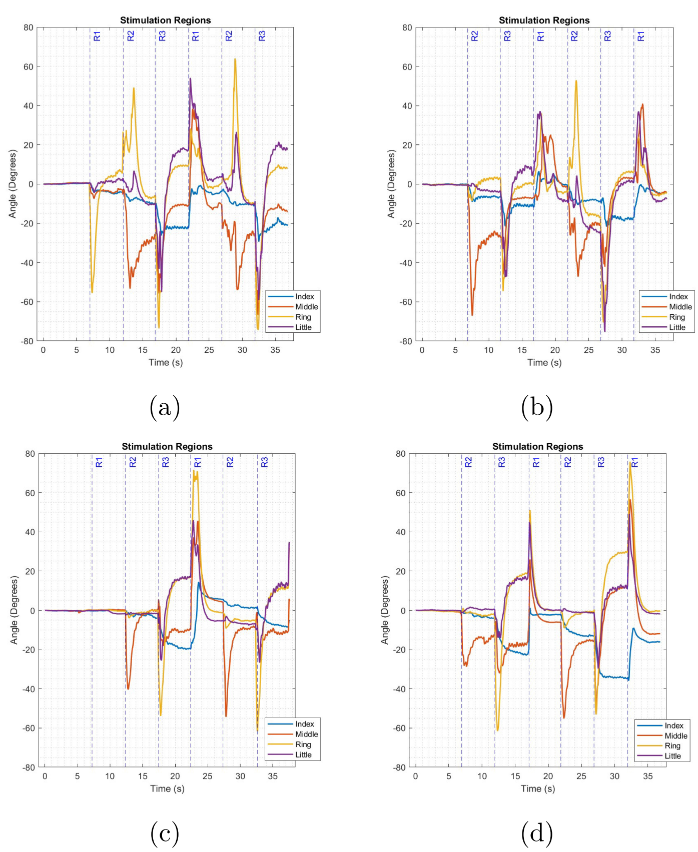

Figure 9. Rotation angles obtained from acceleration sensors attached to the sensitized glove. The movement patterns correspond to sequences $R1 \rightarrow R2 \rightarrow R3$ for (a) and (c), and $R2 \rightarrow R3 \rightarrow R1$ for (b) and (d), and participant #1 with (a) and (b) and #2 with (c) and (d)

For example, in participant #1, stimulation of R2 predominantly caused contraction of the middle finger and relaxation tendencies in the ring and pinky fingers. This pattern was observed in both repetitions of the sequence $R1 \rightarrow R2 \rightarrow R3$ (Figure 9a) and once in the sequence $R2 \rightarrow R3 \rightarrow R1$ (Figure 9b). Stimulation sequences beginning at R2 (from the resting state) did not generate signals associated with ring and pinky finger relaxation. Additionally, stimulation of R3 induced contraction of the ring, middle, and pinky fingers for both sequences in participant #1. Conversely, stimulation of R1 generally exhibited a relaxation effect, particularly when any fingers were previously contracted. This effect was evident in the sequence $R2 \rightarrow R3 \rightarrow R1$ (Figure 9b) and during the second R1 stimulation in the sequence $R1 \rightarrow R2 \rightarrow R3$ (Figure 9b). When stimulation began at R1 (after the resting state, Figure 9a), a contraction movement was observed in the ring finger. The contraction patterns observed in participant #2 were similar to those noted in participant #1.

In summary, the stimulation sequence $R1 \rightarrow R2 \rightarrow R3$ (Figure 9c) elicited the following pattern of movements: no finger contraction (R1) → predominant contraction of the middle finger (R2) → predominant contraction of the ring finger, with less pronounced contractions of the middle and pinky fingers (R3). Conversely, the sequence $R2 \rightarrow R3 \rightarrow R1$ (Figure 9d) produced the following movement pattern: predominant contraction of the middle finger (R2) → predominant contraction of the ring finger, along with less pronounced contractions of the middle and pinky fingers (R3) → no contraction or relaxation of previously contracted fingers (R1). Predominant contraction events for both participants and stimulation sequences are summarized in Table 1.

Table 1. Summary of finger contractions or relaxing events for two stimulation sequences in both participants ($P\#1, P\#2$).

Seq	R1 → R2 → R3			R2 → R3 → R1		
P#1	ring - - -	middle - - -	ring mean/ little	middle - - -	ring mean/ little	relaxing - - -
P#2	relaxing - - -	middle - - -	ring mean/ little	middle - - -	ring mean/ little	relaxing - - -

4. Conclusions

This study presents a prototype for a Functional Electrical Stimulation (FES) multichannel system capable of delivering programmable sequences of multiplexed rectangular biphasic signals across four isolated channels, with operational control via a smartphone.

The proposed prototype offers several technological and documentation advancements compared to prior research on similar electrical stimulation technologies. First, the current design employs the widely accessible, cost-effective, and well-supported ESP32 wireless microcontroller. This modern controller simplifies the stimulator's electronic control block, addressing limitations in earlier designs that relied on outdated controllers, as noted in [15], [20]. This modification provides a replicable alternative for the control block of stimulation technologies, potentially facilitating further research in artificial motor control. Second, this study provides detailed performance data for the circuitry within the stimulus generation block, a feature not addressed in prior designs of multichannel electrical stimulators [15], [20].Specifically, the current output exhibited a strong dependence on the adjustment of resistors RAdj and Rvg (Figure 3). While the circuit effectively generates constant current stimuli, the maximum current level and the dynamic range of the amplifier stage are constrained by increases in the load magnitude connected to the output. Third, this prototype introduces a scalable multiplexing scheme utilizing a combination of optocoupler and trial per channel. This topology enables straightforward replication to expand the number of channels as needed.

Additionally, the preliminary tests demonstrated the system's capability to generate programmable sequences of controlled muscle contractions.

The results suggest that the prototype is well-suited for integration into extended experimental protocols for multichannel sequential muscle stimulation. Future work will focus on developing a miniaturized, embedded version of the prototype in the form of a handheld device equipped with an accelerometer. This enhanced iteration will facilitate broader experimental applications of multichannel sequential muscle stimulation, including studies on its impact on conditions such as Parkinson's disease and stroke.

References

[1] R. N. L. Lamptey, B. Chaulagain, R. Trivedi, A. Gothwal, B. Layek, and J. Singh, "A review of the common neurodegenerative disorders: Current therapeutic approaches and the potential role of nanotherapeutics," *International Journal of Molecular Sciences*, vol. 23, no. 3, 2022. [Online]. Available: https://doi.org/10.3390/ijms23031851

[2] C. H. Zapata-Zapata, E. Franco-Dáger, J. M. Solano-Atehortúa, and L. F. Ahunca-Velásquez, "Esclerosis lateral amiotrófica: actualización," *Revista Médica Iatreia*, vol. 29, no. 2, pp. 194–205, 2016. [Online]. Available: https://doi.org/10.17533/udea.iatreia.v29n2a08

[3] N. Cardona, S. J. Ocampo, J. M. Estrada, M. I. Mojica, and G. L. Porras, "Caracterización clínica y funcional de pacientes con atrofia muscular espinal en el centro-occidente colombiano,"

Revista del Instituto Nacional de Salud Biomedica, vol. 42, no. 1, pp. 59–99, 2022. [Online]. Available: https://doi.org/10.7705/biomedica.6178

[4] L. Meng, M. Jin, X. Zhu, and D. Ming, "Peripherical electrical stimulation for parkinsonian tremor: A systematic review," *Frontiers in Aging Neuroscience*, vol. 14, 2022. [Online]. Available: https://doi.org/10.3389/fnagi.2022.795454

[5] O. Hardiman, A. Al-Chalabi, A. Chio, E. M. Corr, G. Logroscino, W. Robberecht, P. J. Shaw, Z. Simmons, and L. H. van den Berg, "Amyotrophic lateral sclerosis," *Nature Reviews Disease Primers*, vol. 3, no. 1, p. 17071, Oct 2017. [Online]. Available: https://doi.org/10.1038/nrdp.2017.71

[6] M. Gobbo, S. Lazzarini, L. Vacchi, P. Gaffurini, L. Bissolotti, A. Padovani, and M. Filosto, "Exercise combined with electrotherapy enhances motor function in an adolescent with spinal muscular atrophy type iii," *Case Reports in Neurological Medicine*, vol. 2019, no. 1, p. 4839793, 2019. [Online]. Available: https://doi.org/10.1155/2019/4839793

[7] A. Wright and K. A. Sluka, "Nonpharmacological treatments for musculoskeletal pain," *The Clinical Journal of Pain*, vol. 17, no. 1, 2001. [Online]. Available: https://doi.org/10.1097/00002508-200103000-00006

[8] D. B. Popovic, "Advances in functional electrical stimulation (fes)," *Journal of Electromyography and Kinesiology*, vol. 24, no. 6, pp. 795–802, 2014. [Online]. Available: https://doi.org/10.1016/j.jelekin.2014.09.008

[9] C. Marquez-Chin and M. R. Popovic, "Functional electrical stimulation therapy for restoration of motor function after spinal cord injury and stroke: a review," *BioMedical Engineering OnLine*, vol. 19, no. 1, p. 34, May 2020. [Online]. Available: https://doi.org/10.1186/s12938-020-00773-4

[10] M. Djurić-Jovičić, S. Radovanović, I. Petrović, C. Azevedo, G. Mann, and M. Popović, "The impact of functional electrical stimulation (fes) on freezing of gait (fog) in patients with parkinson's disease," *Clinical Neurophysiology*, vol. 124, no. 7, p. e11, 2013. [Online]. Available: https://doi.org/10.1016/j.clinph.2012.12.019

[11] F. Naz, D. Hussain, H. Ali, Q. Raza, and F. Siddique, "Effectiveness of functional electrical stimulation machine in managing neurological diseases - a retrospective study," *Pakistan Journal of Medical Sciences*, vol. 40, no. 2(ICON), Dec. 2023. [Online]. Available: https://doi.org/10.12669/pjms.40.2(ICON).8966

[12] R. Rupp and H. J. Gerner, *Neuroprosthetics of the upper extremity — clinical application in spinal cord injury and challenges for the future*. Vienna: Springer Vienna, 2007, pp. 419–426. [Online]. Available: https://doi.org/10.1007/978-3-211-33079-1_55

[13] W. Young, "Electrical stimulation and motor recovery," *Cell Transplantation*, vol. 24, no. 3, pp. 429–446, 2015, pMID: 25646771. [Online]. Available: https://doi.org/10.3727/096368915X686904

[14] A. Masdar, B. K. K. Ibrahim, and M. M. Abdul Jamil, "Development of wireless-based low-cost current controlled stimulator for patients with spinal cord injuries," in *2012 IEEE-EMBS Conference on Biomedical Engineering and Sciences*, 2012, pp. 493–498. [Online]. Available: https://doi.org/10.1109/IECBES.2012.6498175

[15] H.-P. Wang, A.-W. Guo, Y.-X. Zhou, Y. Xia, J. Huang, C.-Y. Xu, Z.-H. Huang, X.-Y. Lü, and Z.-G. Wang, "A wireless wearable surface functional electrical stimulator," *International Journal of Electronics*, vol. 104, no. 9, pp. 1514–1526, 2017. [Online]. Available: https://doi.org/10.1080/00207217.2017.1312708

[16] T. Keller, M. Lawrence, A. Kuhn, and M. Morari, "New multi-channel transcutaneous electrical stimulation technology for rehabilitation," in *2006 International Conference of the IEEE Engineering in Medicine and Biology Society*, 2006, pp. 194–197. [Online]. Available: https://doi.org/10.1109/IEMBS.2006.259399

[17] S. V. C. y Jose Hernandez Jacquez y Mario Cepeda Rubio y Carlos Juárez Rodríguez y Diana Piña Santos y Geshel Guerrero Lopez, "Efecto de los electroestimuladores tens en los síntomas motores de la enfermedad de parkinson," *Medicina e Investigación Universidad Autónoma del Estado de México*, vol. 11, no. 1, pp. 1–5, 2023. [Online]. Available: https://doi.org/10.36677/medicinainvestigacion.v11i1.20293

[18] F. C. Atamaz, B. Durmaz, M. Baydar, O. Y. Demircioglu, A. Iyiyapici, B. Kuran, S. Oncel, and O. F. Sendur, "Comparison of the efficacy of transcutaneous electrical nerve stimulation, interferential currents, and shortwave diathermy in knee osteoarthritis: A double-blind, randomized, controlled, multicenter study," *Archives of Physical Medicine and Rehabilitation*, vol. 93, no. 5, pp. 748–756, 2012. [Online]. Available: https://doi.org/10.1016/j.apmr.2011.11.037

[19] S. Farahmand, H. Vahedian, M. Abedinkhan Eslami, and A. M. Sodagar, "Wearable, battery-powered, wireless, programmable

8-channel neural stimulator," in *2012 Annual International Conference of the IEEE Engineering in Medicine and Biology Society*, 2012, pp. 6120–6123. [Online]. Available: https://doi.org/10.1109/EMBC.2012.6347390

[20] Q. Xu, T. Huang, J. He, Y. Wang, and H. Zhou, "A programmable multi-channel stimulator for array electrodes in transcutaneous electrical stimulation," in *The 2011 IEEE/ICME International Conference on Complex Medical Engineering*, 2011, pp. 652–656. [Online]. Available: https://doi.org/10.1109/ICCME.2011.5876821

[21] M. Sugandi, H. Satria, H. Arif, N. Nelmiawati, and I. H. Mulyadi, "Low cost wireless ecg patch using esp32," *Journal Integrasi*, vol. 12, no. 1, pp. 31–35, 2020. [Online]. Available: https://doi.org/10.30871/ji.v12i1.1764

[22] J. Ferdous, B. Roy, M. Hossen, and M. I. Md., "Implementation of iot based patient health monitoring system using esp32 web server," *International Journal of Advanced Research (IJAR)*, vol. 11, pp. 716–726, 2023. [Online]. Available: https://dx.doi.org/10.21474/IJAR01/17119

[23] K. Sangeethalakshmi, A. S. Preethi, U. Preethi, S. Pavithra, and P. V. Shanmuga, "Patient health monitoring system using iot," *Materials Today: Proceedings*, vol. 80, pp. 2228–2231, 2023, sI:5 NANO 2021. [Online]. Available: https://doi.org/10.1016/j.matpr.2021.06.188

[24] R. Priyanka and M. Reji, "Iot based health monitoring system using blynk app," *International Journal of Engineering and Advanced Technology (IJEAT=*, vol. 8, no. 6, pp. 78–81, 2019. [Online]. Available: http://www.doi.org/10.35940/ijeat.E7467.088619

[25] Kodular. (2023) Home – kodular. [Online]. Available: https://upsalesiana.ec/ing33ar4r25

[26] M. D. E. Goodyear, K. Krleza-Jeric, and T. Lemmens, "The declaration of helsinki," *BMJ*, vol. 335, no. 7621, pp. 624–625, 2007. [Online]. Available: https://doi.org/10.1136/bmj.39339.610000.BE

[27] X. Bao, Y. Zhou, Y. Wang, J. Zhang, X. Lü, and Z. Wang, "Electrode placement on the forearm for selective stimulation of finger extension/flexion," *PLOS ONE*, vol. 13, no. 1, pp. 1–22, 01 2018. [Online]. Available: https://doi.org/10.1371/journal.pone.0190936

[28] A. Takahashi, J. Brooks, H. Kajimoto, and P. Lopes, "Increasing electrical muscle stimulation's dexterity by means of back of the hand actuation," in *Proceedings of the 2021 CHI Conference on Human Factors in Computing Systems*, ser. CHI '21. New York, NY, USA: Association for Computing Machinery, 2021. [Online]. Available: https://doi.org/10.1145/3411764.3445761